

NMR and NQR study of the tetrahedral frustrated quantum spin system $\text{Cu}_2\text{Te}_2\text{O}_5\text{Br}_2$ in its paramagnetic phase

Arnaud Comment,* Hadrien Mayaffre, Vesna Mitrović,† Mladen Horvatić, and Claude Berthier
*Laboratoire National des Champs Magnétiques Intenses,
CNRS UPR3228, Université J. Fourier,
BP166 38042 Grenoble, France*

Béatrice Grenier
INAC, SPSMS, CEA, F-38042 Grenoble, France

Patrice Millet
Centre d'Elaboration de Matériaux et d'Etudes Structurales, CEMES/CNRS, F-31062 Toulouse, France
(Dated: March 4, 2022)

The quantum antiferromagnet $\text{Cu}_2\text{Te}_2\text{O}_5\text{Br}_2$ was investigated by NMR and NQR. The ^{125}Te NMR investigation showed that there is a magnetic transition around 10.5 K at 9 T, in agreement with previous studies. From the divergence of the spin-lattice relaxation rate, we ruled out the possibility that the transition could be governed by a one-dimensional divergence of the spin-spin correlation function. The observed anisotropy of the ^{125}Te shift was shown to be due to a spin polarization of the $5s^2$ “E” doublet of the $[\text{TeO}_3\text{E}]$ tetrahedra, highlighting the importance of tellurium in the exchange paths. In the paramagnetic state, Br NQR and NMR measurements led to the determination of the Br hyperfine coupling and the electric field gradient tensor, and to the spin polarization of Br p orbitals. The results demonstrate the crucial role of bromine in the interaction paths between Cu spins.

PACS numbers: 76.60.k, 75.30.m, 75.10.Jm

I. INTRODUCTION

In quantum antiferromagnets, triangular or tetrahedral coordination generates strong frustration. Unusual singlet ground states deriving from this frustration have been theoretically predicted and actively searched for in the recent years, mainly on Kagome or pyrochlore systems, in which the frustrated units (triangle or tetrahedra) are sharing corners. A different type of geometry, in which the tetrahedra units are isolated, and only weakly coupled has been discovered with the compounds $\text{Cu}_2\text{Te}_2\text{O}_5\text{X}_2$ ($\text{X} = \text{Br}, \text{Cl}$)¹, which contain tetrahedral clusters of Cu^{2+} ($S = \frac{1}{2}$) in a distorted square planar CuO_3X coordination. These tetrahedra align to form chains along the $[001]$ direction, and are separated along the $[100]$ and $[010]$ directions by different Te-O coordinations². Although the ground state of individual tetrahedron is expected to be a singlet (quasi-0D system), it turns out that, below about 12 K (18 K for the Cl compound), the intertetrahedra couplings lead to an incommensurate magnetic ground state with anomalous thermodynamics properties^{3,4}. To determine relevant dimensionality of the system several different models were considered. These include: quasi-1D ones, assuming an interaction between tetrahedra along the c -axis⁵⁻⁷; quasi-2D consisting of interacting frustrated plaquettes in the ab -plane, in which intertetrahedra couplings are assumed to be important⁸⁻¹⁰; and models of a 3D tetrahedral cluster-spin system^{11,12}. Despite all these studies, the exact dimensionality of the system remains unclear.

Nevertheless, the results of Jensen *et al.* and Jagličić *et al.* appear to favor a 3D over 1D nature of the magnetic transition¹³⁻¹⁵. It is likely that both the intratetrahedral (and thus the frustration), leading to a creation of spin-gaps, and the intertetrahedral interactions, inducing a magnetic long range order, are present and compete together.

One of the important unsettled questions is the relative strength of the various exchange couplings within and between tetrahedra, which determine the dimensionality of the system. In this paper, we present NMR and NQR measurements performed on single crystals of $\text{Cu}_2\text{Te}_2\text{O}_5\text{Br}_2$. The purpose of this study was to address the question of the magnetic phase dimensionality via an investigation in the vicinity of the phase transition and to determine the spin polarization of the Cu ligands. One challenge that came along was the rather intricate assignment of the various NMR transitions possible in this system.

II. TELLURIUM NMR

A. Spectrum structure

Tellurium has two NMR-active isotopes and both have a spin- $\frac{1}{2}$ nucleus, but the natural abundance of ^{125}Te is about 8 times higher than the one of ^{123}Te . For this reason, all Te NMR measurements were performed on ^{125}Te . $\text{Cu}_2\text{Te}_2\text{O}_5\text{Br}_2$ crystalizes in the $P\bar{4}$ ($a = b = 7.8 \text{ \AA}$,

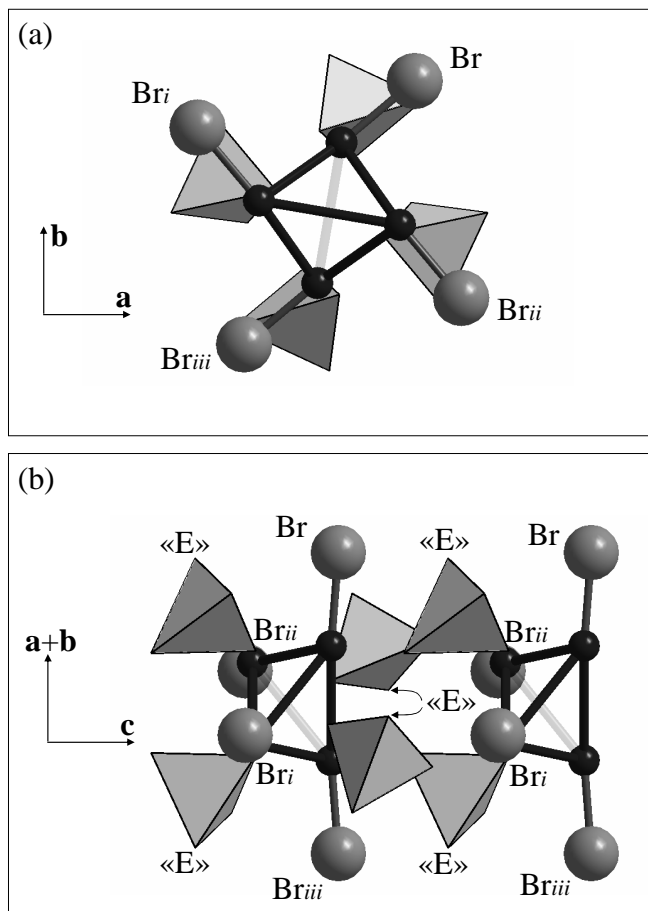


FIG. 1: Schematic views of the $\text{Cu}_2\text{Te}_2\text{O}_5\text{Br}_2$ structure along the $[001]$ axis (a) and the $[\bar{1}10]$ axis (b). Copper atoms (small spheres) are interconnected to emphasize the tetrahedral configuration. Tellurium atoms (not represented) are placed inside the sketched “ O_3E ” tetrahedra, E representing the $5s^2$ lone pair of the Te atom¹.

$c = 6.4 \text{ \AA}$) space group, meaning that the elementary pattern $\text{CuTeO}_{2.5}\text{Br}$ is present four times in each unit cell. As a consequence, although ^{125}Te has a spin- $\frac{1}{2}$ nucleus and therefore yields to a single resonance line, the crystal has four inequivalent Te sites for an arbitrary orientation with respect to the direction of the external magnetic field B_0 . Thus, the ^{125}Te NMR spectrum in $\text{Cu}_2\text{Te}_2\text{O}_5\text{Br}_2$ is generally composed of four lines. However, by applying the field in the ab -plane, two sites become equivalent, while applying it along the c -axis, all four sites become equivalent (see Fig. 1; for a full description of the crystal symmetry, see e.g. the article of Johansson *et al.*¹).

B. Hyperfine shift

The temperature dependence of the electron spin susceptibility of $\text{Cu}_2\text{Te}_2\text{O}_5\text{Br}_2$ has been extensively studied

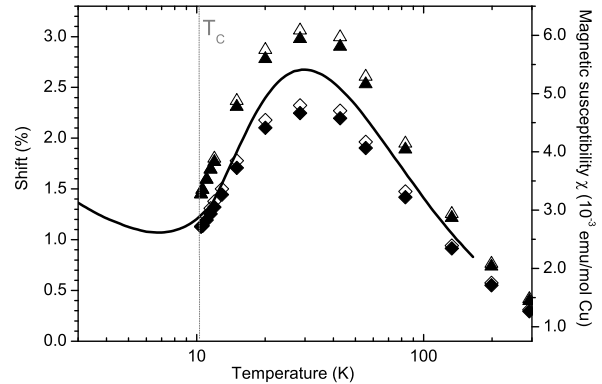


FIG. 2: Temperature dependence of the shift of the four inequivalent ^{125}Te nuclear spins measured in a field of 9 T almost parallel to $[110]$ superimposed to the SQUID susceptibility measurements (line). The existence of four NMR lines is due to a slight misorientation of the field out of the ab -plane

by means of DC and AC susceptometry^{1,2,13,14,16}. NMR measurements provide a way to probe the local electron spin susceptibility through hyperfine interactions with the advantage of being essentially insensitive to paramagnetic impurities. This is of particular interest for probing magnetic systems at low temperature when the contribution from paramagnetic impurities becomes larger than the system intrinsic susceptibility. The temperature dependence of the resonance frequencies, proportional to the macroscopic spin susceptibility, of the four inequivalent ^{125}Te nuclear spins in the crystal and their temperature dependence measured in a field of 9 T parallel to a direction nearly parallel to $[110]$ is shown in Fig. 2. The data is superimposed to the SQUID susceptibility measurements performed with a field of 0.1 T oriented along $[110]$ on the same single crystal.

The data plotted in Fig. 2 allow for the determination of the ^{125}Te hyperfine coupling by comparing the temperature dependence of the NMR frequencies to the temperature dependence of the magnetic susceptibility as shown in Fig. 3. In doing so, we took advantage of the multiple sites, and thus the multiple resonances, to determine the zero-shift frequency as the extrapolated frequency at which all sites have the same resonance frequency, in the present case $f_0 \cong 121.5 \text{ MHz}$. This value corresponds to the ^{125}Te frequency for which the contribution of the Cu electron spins polarization is zero. Note however that it is not the resonance frequency of the “bare” ^{125}Te nuclear spin (121.07 MHz¹⁷) since the Te electron shells also shift (essentially isotropically) the resonance. We observe here that this shift is about 0.35%, which is in the range of the observed shifts in transition-metal tellurides¹⁷. Conjectively, the dependence of the NMR frequencies on the crystal orientation (see Fig. 4) yields to the full determination of the hyperfine tensor. From the data shown in Fig. 4, we deduced that the tellurium hyperfine shift (re-

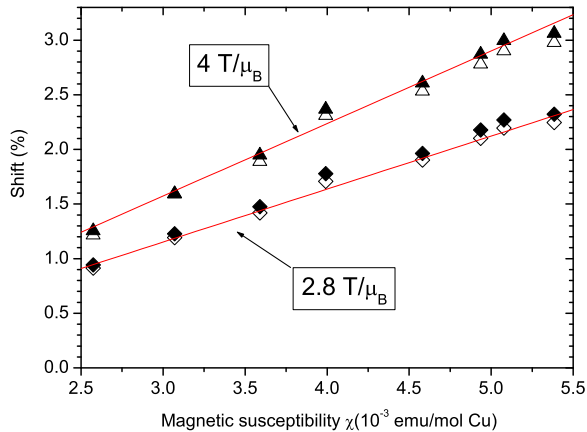


FIG. 3: Linear relationship between the shift of the four inequivalent ^{125}Te nuclear spins measured in a field of 9 T almost parallel to $[110]$ and the SQUID susceptibility. The calculation of the slopes lead to the determination of the hyperfine field.

flecting the spin susceptibility) is mainly isotropic with a small anisotropic part in the ab -plane along a principal axis nearly parallel to the $[110]$ direction. Assuming an environment of axial symmetry (i.e. neglecting a small anisotropy in the plane perpendicular to $[110]$), we can define the hyperfine shift along the external magnetic field \mathbf{B}_0 as $K(\theta) = K_{iso} + K_{ax}(3\cos^2\theta - 1)/2$, where θ is the angle between \mathbf{B}_0 and the principal anisotropy axis of the Knight shift tensor \mathbf{K} , K_{iso} the isotropic part of \mathbf{K} and K_{ax} its anisotropic part along the principal anisotropy axis. The data lead to $K_{iso}=3.2\text{ T}/\mu_B$ and $K_{ax}=0.8\text{ T}/\mu_B$. A simple computation of the dipolar contribution of a single Cu electron spin cannot account for either the amplitude, which is 8 times weaker than the observed value, nor the angular dependence shown in Fig. 4. Considering transferred polarization on Br atoms cannot account for our observations as well. However, the measured angular dependence can be well described by considering the contribution of a Te orbital pointing towards the center of the Br-Br axis (see simulation shown in the inset of Fig. 4). Johnsson *et al.* pointed out that the Te atom is placed at the center of the O_3E tetrahedron, where E represents the $5s^2$ lone pair of the Te atom¹. As shown in Fig.1(b), the “E” apex of the tetrahedron stands in between two bromine atoms along the c -axis and the “E” orbital should therefore point in the $[110]$ direction. Our results thus suggest that part of the spin polarization is located in this orbital. This observation is fully compatible with the description of Johnsson *et al.* who suggest that the “E” orbital participates in the electronic structure binding the two neighboring Br atoms along the c -axis¹.

A quantitative estimation of this contribution is more delicate. First, it should be noted that a nearly axial

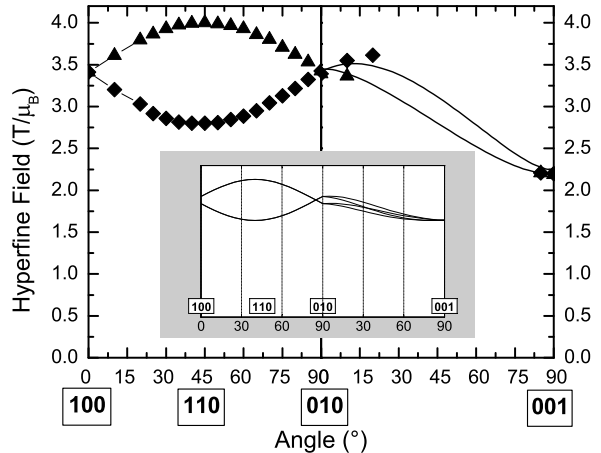


FIG. 4: Crystal orientation dependence of the ^{125}Te hyperfine field measured at 15 K and 9.4 T. The crystal was aligned to obtain only two resonance peaks in the ab -plane (with this orientation, the filled diamonds and the filled triangles in Fig. 2 and Fig. 3 would be indistinguishable from the open diamonds and the open triangles, respectively). Inset: dipolar field calculated for a Te orbital pointing towards the center of the Br-Br axis.

symmetry around the $[110]$ direction is not compatible with a transfer of polarization from the three oxygens forming the tetrahedral environment of the tellurium atom, the “E” orbital being the fourth corner. In order to respect the symmetry, all 3 oxygen atoms should equally contribute, which is highly unlikely as their local environment differs dramatically from one another (see Fig. 5). Assuming that the “E” orbital can be described by a superposition of $5s$ and $5p$ orbitals (the tetrahedral symmetry of tellurium site suggests a sp^3 hybridization) with one sp^3 orbital pointing in the $[110]$ direction, we can write that $K_{ax} = 6/5f_p\mu_B \langle r^{-3} \rangle$, where f_p is the fraction of unpaired electron in the corresponding orbital and $\langle r^{-3} \rangle$ is the mean value of $1/r^3$ over the $5p$ orbital. By taking $\langle r^{-3} \rangle = 104 \cdot 10^{24} \text{ cm}^{-318}$, one finds that $f_p = 0.7\%$. Similarly, from $K_{iso} = 8\pi/3f_s\mu_B \langle |\Psi(0)|^2 \rangle$, with $\langle |\Psi(0)|^2 \rangle$ being the square of the s -wave function at the nucleus averaged over those electrons at the Fermi surface, one can estimate the spin density in the $5s$ contribution to sp^3 orbital to give a contact term consistent with the isotropic spin part. Knowing that in an ideal sp^3 orbital the s contribution is 4 times smaller than in pure s orbital, by taking the value given by Morton¹⁸, i.e. $\langle |\Psi(0)|^2 \rangle = \frac{1}{4} \cdot 170 \cdot 10^{24} \text{ cm}^{-3}$, one finds $f_s = 0.96\%$. This value is nearly identical to the value of f_p determined from dipolar contribution, which confirms this description in terms of sp^3 orbital.

In conclusion, this contribution from the “E” orbital well describes the measurements. In addition, only a small spin polarization is needed in the Te “E” doublet to quantitatively account for the data. One should note

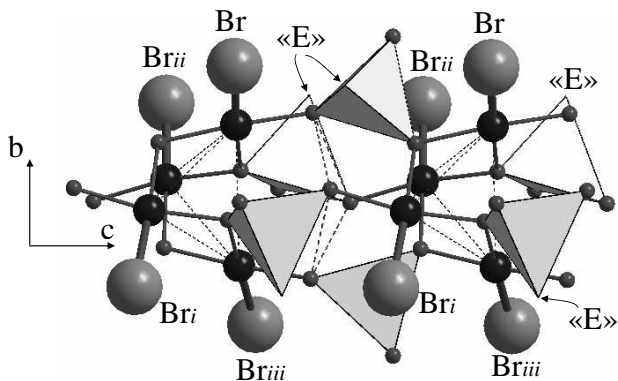


FIG. 5: Schematic view of the $\text{Cu}_2\text{Te}_2\text{O}_5\text{Br}_2$ structure along the $[100]$ axis. Oxygen atoms (smallest spheres) are displayed and dashed lines show the exchange paths proposed by⁹.

that this interpretation is not compatible with the model proposed by Whangbo *et al.* in which the interactions between tetrahedral clusters are presumably from two types of super-superexchange paths⁹: one is Cu-O-O-Cu path in the c direction and the other Cu-Br-Br-Cu path in the ab -plane with a path Cu-Br-Br-Cu⁹. Our results suggest that the relevant path is Cu-Br-“E”-Br-Cu in the c direction.

C. Magnetic phase transition

It has been reported in an earlier study that the system undergoes a magnetic transition at a temperature T_C of about 12 K in an external magnetic field of 9 T². In the present study, we observe that the ^{125}Te resonance line suddenly disappears, as the temperature is lowered towards T_C . Although it was possible to observe the resonance at temperatures very close to $T_C = 12$ K, we were not able to observe the signal at temperatures below the magnetic transition temperature. This might be due to a significant broadening of the line, a strong shortening of the spin-spin relaxation time, a very large frequency shift or possibly a combination of these effects.

The temperature dependence of the ^{125}Te spin-lattice relaxation time measured on the lowest-frequency resonance in a field of 9 T along a direction nearly parallel to $[110]$ is shown in Fig. 6. The ^{125}Te spin-lattice relaxation rate decreases with decreasing temperature for temperatures below 100 K, but abruptly increases around 12 K. Such a dramatic change in spin-lattice relaxation rate is an evidence for strong local field fluctuations and therefore for a magnetic transition. The occurrence of a divergence in the ^{125}Te spin-lattice relaxation rate within a narrow region of a few K above T_C unambiguously shows the three-dimensional character of the magnetic system. In a quasi-one-dimensional system, the fluctuations would extend on a temperature range comparable to T_C . The transition temperature deduced from these measurements is $T_C = 10.5$ K, which is slightly lower than

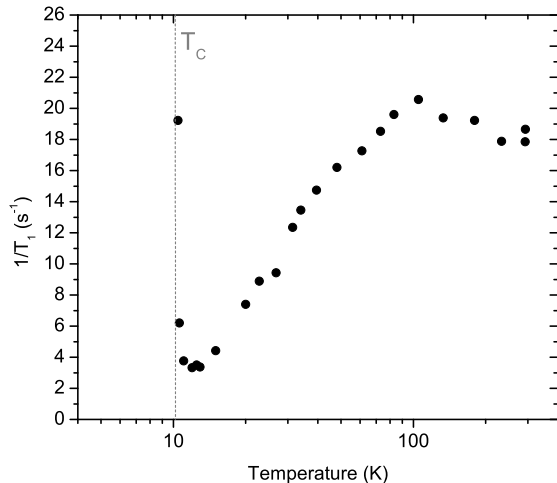


FIG. 6: Temperature dependence of the ^{125}Te spin-lattice relaxation rate measured at 9 T on the lowest-frequency resonance (filled diamonds in Fig. 2 and Fig. 3).

TABLE I: Spin, natural abundance, gyromagnetic ratio, electric quadrupole moment²¹, and measured nuclear quadrupole frequencies of the two bromine isotopes.

	Spin	Nat. abund. (%)	$\gamma_n/2\pi$ (MHz/T)	Q (barn)	$\nu_{NQR,15K}$ (MHz)
^{79}Br	3/2	50.69	10.7	0.313	87.41
^{81}Br	3/2	49.31	11.53	0.262	73.02

the value determined by Lemmens *et al.*².

III. BROMINE NMR AND NQR IN THE PARAMAGNETIC STATE

Halogen nuclei have a large quadrupole moment and they have been extensively studied by nuclear quadrupole resonance (NQR)¹⁹. NQR frequencies strongly depend on the ionic character of the M-X bond where M is a metal ion and X is the halogen ion²⁰. Both bromine isotopes have a spin-3/2 nucleus and ^{79}Br and ^{81}Br have almost equivalent natural abundance (Br nuclear properties are summarized in Table I). $\text{Cu}_2\text{Te}_2\text{O}_5\text{Br}_2$ contains tetrahedral arrangements of Cu atoms each one of them placed at the center of a distorted square CuO_3Br . As shown in Fig. 1 (see also¹), copper-bromine bonds are almost perpendicular to the c -axis of the crystal (90 ± 4.42 degrees). While Cu-Br and $\text{Cu}_{iii}\text{-Br}_{iii}$ are nearly parallel to the $[110]$ direction, $\text{Cu}_i\text{-Br}_i$ and $\text{Cu}_{ii}\text{-Br}_{ii}$ are nearly parallel to the $[\bar{1}10]$ one. As for tellurium, there are four inequivalent Br sites, which reduce to two inequivalent sites when the direction of B_0 is in the ab -plane, and to one single site if B_0 is parallel to the c -axis.

The total Hamiltonian of a Br nuclear spin in the $\text{Cu}_2\text{Te}_2\text{O}_5\text{Br}_2$ paramagnetic phase can be written as

$$\hat{\mathcal{H}} = -\gamma_n \hbar \mathbf{B}_0 \cdot \mathbf{I} - \gamma_n \hbar \mathbf{B}_0 \cdot \mathbf{K} \cdot \mathbf{I} + \frac{eQ}{2I(2I-1)} \mathbf{I} \cdot \mathbf{V} \cdot \mathbf{I}, \quad (1)$$

where the first term is the nuclear Zeeman Hamiltonian, the second term is the hyperfine Hamiltonian with \mathbf{K} the Knight shift tensor, and the third term is the quadrupole Hamiltonian, in which e is the elementary charge, Q is the quadrupole moment and \mathbf{V} is the electric field gradient (EFG) tensor. In its principal axis coordinate system (X, Y, Z), the electric field gradient is diagonal and traceless. In this particular frame, Eq. 1 can be rewritten as

$$\hat{\mathcal{H}} = -\gamma_n \hbar \mathbf{B}_0 \cdot \mathbf{I} - \gamma_n \hbar \mathbf{B}_0 \cdot \mathbf{K} \cdot \mathbf{I} + \frac{1}{6} \nu_Q [3I_Z^2 - I(I+1) + \frac{\eta}{2}(I_+^2 + I_-^2)], \quad (2)$$

where $\eta = (V_{XX} - V_{YY})/V_{ZZ}$ is the asymmetry parameter of the electric field gradients, and $I_+ = I_X + iI_Y$ and $I_- = I_X - iI_Y$ are the spin raising and lowering operators. For $I = 3/2$, $\nu_Q = \nu_{NQR}(1 + \eta^2/3)^{-1/2}$, where ν_{NQR} is the pure quadrupole resonance frequency.

At 15 K and in the absence of applied static magnetic field \mathbf{B}_0 , we observed two lines of identical intensity, one at ${}^{79}\nu_{NQR} = 87.41$ MHz corresponding to the ${}^{79}\text{Br}$ quadrupole resonance, and the other at ${}^{81}\nu_{NQR} = 73.02$ MHz corresponding to that of ${}^{81}\text{Br}$ (see Fig. 7). These values are in agreement with the ratio of the nuclear quadrupole moments published in the literature²². Given the gyromagnetic ratio of the two bromine isotopes (c.f. Table I), it is clear that the high-field approximation, which consists in considering the quadrupole interaction as a perturbation to the Zeeman one, will not yield to the correct transition energies for standard NMR field values. Unlike in the case of a Zeeman only or a quadrupole only Hamiltonian, the eigenvectors of the total Hamiltonian are not pure and therefore the so-called forbidden transitions can have a non-zero probability of occurring. For $I = 3/2$, the six possible transitions between the different available spin states are shown in Fig. 8(a). As a consequence, analytical solutions cannot be calculated and a numerical computation is required.

For the present study, we developed a MATLAB routine to calculate the field dependence of the resonance frequencies and their associated intensities for Br sites in an arbitrary orientation of the field. The code was written such as to numerically diagonalize the Hamiltonian described in Eq. 2, compute the resonance frequencies from its eigenvalues and determine the expected relative intensity of each transition by calculating $|\langle \varphi_i | \gamma_n \hbar \mathbf{B}_1 \cdot \mathbf{I} | \varphi_j \rangle|^2$, $i \neq j$, where \mathbf{B}_1 is the radio-frequency excitation field created in the NMR coil and φ_i, φ_j are eigenstates of the Hamiltonian. In the x, y, z laboratory frame, $\mathbf{B}_1 \cdot \mathbf{I}$ can be expressed in terms of the X, Y, Z projections of \mathbf{I} using two Euler angles, Ω and Ψ defined in Fig. 8(b)), giving $\mathbf{B}_1 \cdot \mathbf{I} =$

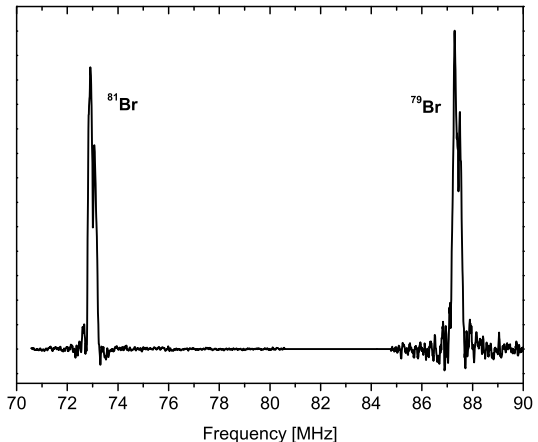


FIG. 7: Br NQR spectrum measured at 15 K. The intensities have been divided by the square of the frequency. Note that the slight splitting observed on both lines is due to the presence of a residual non-zero \mathbf{B}_0 field in the superconducting coil.

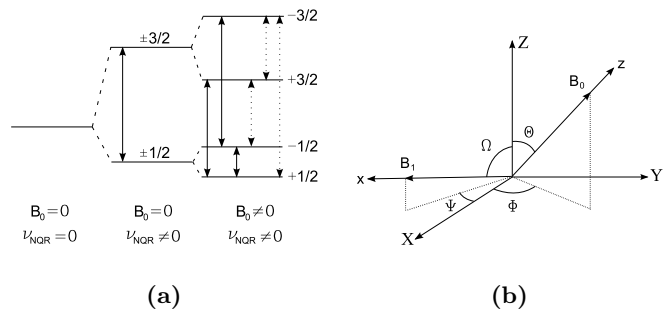


FIG. 8: (a) Sketch of the energy levels of Br nuclei. The solid arrows are the $\Delta m = 1$ transitions and the dotted ones the $\Delta m > 1$ transitions (b) Definition of angles Θ , Φ , Ω , and Ψ . The X, Y, Z axes correspond to the principal axes of the EFG and Knight shift tensors.

$B_1(I_X \sin \Omega \cos \Psi + I_Y \sin \Omega \sin \Psi + I_Z \cos \Omega)$. The magnitude of the transition probabilities will thus strongly depend on the intensity of \mathbf{B}_0 as well as on its direction in the X, Y, Z frame, i.e. on the crystal orientation. This is particularly important in the present study where the Zeeman and quadrupolar terms are of comparable magnitude.

Having determined the bromine NQR frequencies by experiment, the remaining unknown parameters in the Hamiltonian given in Eq. 2 are the Knight shift tensor, the orientation of the EFG tensor principal axes with respect to the crystal axes and the associated asymmetry parameter η . Several frequency and field scans were performed in the range 10 to 220 MHz and 5 to 15 T, respectively, with field applied along 4 different directions,

namely [100], [110], [210], and [001]. As an example, a frequency scan performed with $B_0=14$ T applied along [110] is shown in Fig. 9. The computed NMR frequencies and associated intensities calculated for various η values with $\mathbf{K} = \mathbf{0}$ were compared to the measurements. We concluded that the Z -axes of the local EFG tensors are along the Cu-Br bonds, one of which being oriented along a direction close to [110] (its exact direction is [1 0.8384 -0.0124]). In addition, a largely anisotropic Knight shift tensor with its Z -axis also parallel to the Cu-Br bonds needed to be introduced in the Hamiltonian in order to match the computed frequencies with the measured ones. Furthermore, up to the precision of our measurements, we deduced that \mathbf{K} is isotropic in the $X - Y$ plane perpendicular to the Cu-Br bond. To simplify the Hamiltonian, we defined the X - and Y -axes to be parallel to the X - and Y -axes of the EFG tensor. It was then possible to perform experiments to fully determine the Knight shift tensor. Indeed, for \mathbf{B}_0 applied along a Cu-Br bond, that is [1 0.8384 -0.0124], the temperature dependence of the Br resonance frequencies leads to the determination of K_{ZZ} . Similarly, $K_{XX} = K_{YY}$ can be determined by applying \mathbf{B}_0 perpendicular to a Cu-Br bond and measuring the temperature dependence of the Br resonances. By comparing these measurements to the temperature dependence of the macroscopic susceptibility, we obtained $K_{ZZ} = 12\text{T}/\mu_B$ and $K_{XX} = K_{YY} = 0.97\text{T}/\mu_B$ (see Fig. 10). From $K_{ZZ} = 8/5f_p\mu_B < r^{-3} >$, with $< r^{-3} > = 103 \cdot 10^{24}\text{cm}^{-3}$, the experimental K_{ZZ} value leads to $f_p = 4.8\%$ along the Z -axis. Such a rather large value of f_p indicates that the bromine ligands are involved in the exchange path between Cu spins.

To determine the only remaining unknown parameter η , we used a modified version of the MATLAB routine designed to minimize the difference between the measured resonance frequencies and fields, and the fitted frequencies and fields with η as free parameter. This led to $\eta = 0.25 \pm 0.01$. It should be noted that we had to take into account a slight misalignment of the crystal in the coil since a tilt of just one degree away from a specific direction results in dramatic frequency shifts. In Fig. 11, we plot the results of simulations for B_0 aligned along a direction close to [110] (the precise direction is [1 1 -0.08] and corresponds to an experimental crystal orientation, which was estimated from the comparison between the measurements shown in Fig. 9 and the calculations). The field dependence of the 48 transitions of the 2 bromine isotopes located on the 4 inequivalent sites are plotted. The calculated intensities are shown on a color scale shown on the right of the figure. On top of the calculated transitions, horizontal and vertical bars are sketched at the frequencies, respectively fields, of the observed resonances measured at fixed field (9 T and 14 T), respectively fixed frequency (110 MHz). The bars reported at 14 T correspond to the measurements shown in Fig. 9.

Although it was not the purpose of the present work to detect all the transitions, many of them had to be

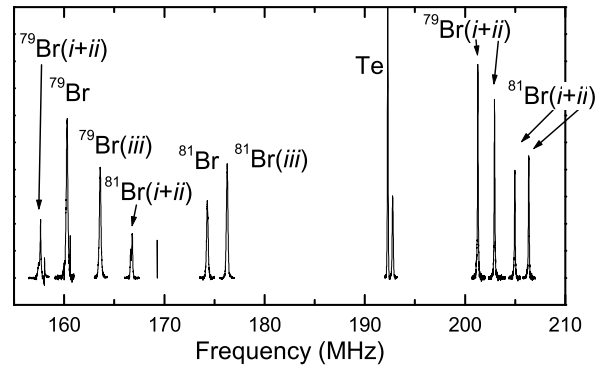


FIG. 9: NMR Spectra for $B_0 = 14$ T along [110]. The intensities have been divided by the square of the frequency. Each line has been identified. The two sharp lines, one around 158 MHz and the other around 169 MHz indicate the position of the ^{63}Cu and ^{65}Cu resonance of the copper NMR coil and have been used to determine the exact value of B_0 . At low frequencies (150-180 MHz) we can find the 8 central lines. For Br_i and Br_{ii} these lines are overlapping since shift and quadrupolar frequency are small in this orientation of the field and the misorientation is not sufficient to separate them. At high frequencies (200-210 MHz), we observe only the four high frequency satellites of Br_i and Br_{ii} . Low frequency satellites are expected below 100 MHz and Br and Br_{iii} high frequency satellites are expected around 240 MHz. Note that since the field direction is close to the principal axis of the EFG tensor, the contribution of the quadrupolar term to the resonance frequency is nearly maximum).

measured in order to correctly interpret the data and to accurately determine the unknown parameters in the Hamiltonian. The observed line intensity ratios do not exactly match the calculated intensity ratios. The reason for this discrepancy is related to the large variations and short spin-spin relaxation times (typically on the order of 5-15 μs at 15 K). It should also be noted that the field dependence of the NMR frequencies of a spin 3/2 with large quadrupolar couplings placed in a strong external field has already been numerically calculated using the Liouvillian formalism and the results were compared to measurements performed in a ^{35}Cl -sodium chlorate NMR study²³. However, the intensity ratios of the transitions were not computed in this previous study.

IV. CONCLUSIONS

The temperature dependence of the Te NMR relaxation rate clearly demonstrates the three-dimensional nature of the magnetic phase transition. This implies that intertetrahedral interactions along the c -axis as well as those in the ab -plane are important. The transition temperature was found to be 10.5 K at 9 T. A Br NMR and NQR study in the paramagnetic phase of $\text{Cu}_2\text{Te}_2\text{O}_5\text{Br}_2$

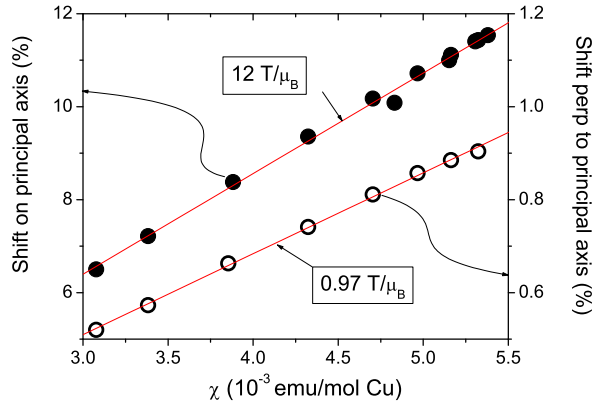


FIG. 10: Br hyperfine shift vs. magnetic susceptibility with T as an implicit parameter. NMR shifts were measured on ^{79}Br at 9 T between 12 and 50 K. Black dots correspond to K_{zz} , parallel to the Cu-Br bond, and open circles to $K_{xx} = K_{yy}$.

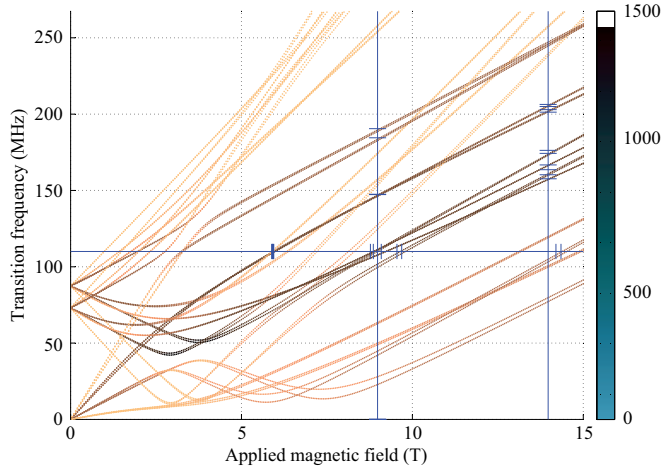


FIG. 11: Computed Br transition frequencies and intensities as a function of the external magnetic field amplitude $|\mathbf{B}_0|$ for \mathbf{B}_0 oriented along $[110]$. The 48 possible transitions for the two Br isotopes and the four inequivalent sites are drawn. The intensities are represented on a color scale in arbitrary units: the lighter the color, the weaker the intensity. The experimental points corresponding to observed transitions are denoted by horizontal tips for spectra recorded at constant field and variable frequencies and by vertical tips for spectra recorded at fixed frequency sweeping the magnetic field.

allowed us to demonstrate the important role of bromine in the interaction paths between Cu spins. In addition, via tellurium NMR, we showed that the $[\text{TeO}_3\text{E}]$ tetrahedra participates in binding the Br atoms.

The theoretical modelization of this frustrated spin system, topic of several recent publications, will be clearly facilitated by this new information. A complete NMR study of this material in its magnetic phase is currently in progress and is expected to shed light on its complex magnetic phase.

Acknowledgments

This work was supported by the French ANR Grant No. 06-BLAN- 0111. We thank Frédéric Mila and Valeri N. Kotov for helpful discussions.

* Electronic address: arnaud.comment@epfl.ch; Present address: Laboratory for functional and metabolic imaging, Ecole Polytechnique Fédérale de Lausanne, CH-1015 Lausanne, Switzerland.

† Present address: Department of Physics, Brown University, Providence, RI 02912.

¹ M. Johansson, K. W. Toernross, F. Mila, and P. Millet, Chem. Mater. **12**, 2853 (2000).

² P. Lemmens, K.-Y. Choi, E. E. Kaul, C. Geibel, K. Becker, W. Brenig, R. Valenti, C. Gros, M. Johansson, P. Millet, et al., Phys. Rev. Lett. **87**, 227201 (2001).

³ O. Zaharko, A. Daoud-Aladine, S. Streule, J. Mesot, P.-J. Brown, and H. Berger, Phys. Rev. Lett. **93**, 217206 (2004).

⁴ O. Zaharko, H. Rønnow, J. Mesot, S. J. Crowe, D. M. Paul, P. J. Brown, A. Daoud-Aladine, A. Meents, A. Wagner, M. Prester, et al., Phys. Rev. B **73**, 064422 (2006).

- ⁵ W. Brenig and K. W. Becker, Phys. Rev. B **64**, 214413 (2001).
- ⁶ K. Totsuka and H.-J. Mikeska, Phys. Rev. B **66**, 054435 (2002).
- ⁷ C. Gros, P. Lemmens, M. Vojta, R. Valenti, K.-Y. Choi, H. Kageyama, Z. Hiroi, N. V. Mushnikov, T. Goto, M. Johnsson, et al., Phys. Rev. B **67**, 174405 (2003).
- ⁸ V. N. Kotov, M. E. Zhitomirsky, and O. P. Sushkov, Phys. Rev. B **63**, 064412 (2001).
- ⁹ M.-H. Whangbo, H.-J. Koo, and D. Dai, Inorg. Chem. **42**, 3898 (2003).
- ¹⁰ V. N. Kotov, M. E. Zhitomirsky, M. Elhajal, and F. Mila, Phys. Rev. B **70**, 214401 (2004).
- ¹¹ W. Brenig, Phys. Rev. B **67**, 064402 (2003).
- ¹² R. Valenti, T. Saha-Dasgupta, C. Gros, and H. Rosner, Phys. Rev. B **67**, 245110 (2003).
- ¹³ J. Jensen, P. Lemmens, and C. Gros, Europhys. Lett. **64**, 689 (2003).
- ¹⁴ Z. Jagličić, S. E. Shawish, A. Jeromen, A. Bilušić, A. Smontara, Z. Trontelj, J. Bonča, J. Dolinšek, and H. Berger, Phys. Rev. B **73**, 214408 (2006).
- ¹⁵ J. Jensen, Phys. Rev. B **79**, 014406 (2009).
- ¹⁶ M. Prester, A. Smontara, I. Živković, A. Bilušić, D. Drobac, H. Berger, and F. Bussy, Phys. Rev. B **69**, 180401 (2004).
- ¹⁷ I. Orion, J. Rocha, S. Jobic, V. Abadie, R. Brec, C. Fernandez, and J.-P. Amoureux, J. Chem. Soc., Dalton Trans. **20**, 3741 (1997).
- ¹⁸ J. R. Morton and K. F. Preston, J. Magn. Res. **30**, 577 (1978).
- ¹⁹ E. A. C. Lucken, *Nuclear Quadrupole Coupling Constants* (Academic Press, London and New York, 1969).
- ²⁰ P. Morgen and W. W. Filho, J. Chem. Phys. **62**, 2183 (1975).
- ²¹ *CRC Handbook of Chemistry and Physics* (CRC Press, 2003), 84th ed.
- ²² R. E. Alonso, A. Svane, C. O. Rodriguez, and N. E. Christensen, Phys. Rev. B **69**, 125101 (2004).
- ²³ M. Khasawneh, J. S. Hartman, and A. D. Bain, Molec. Phys. **102**, 975 (2004).